

1 **Improving Air Quality Model Predictions of Organic Species using**
2 **Measurement-Derived Organic Gaseous and Particle Emissions in a**
3 **Petrochemical-Dominated Region**

4
5 Craig A Stroud¹, Paul A Makar¹, Junhua Zhang¹, Michael D. Moran¹, Ayodeji Akingunola¹,
6 Shao-Meng Li¹, Amy Leithead¹, Katherine Hayden¹, and May Siu²

7
8 ¹Air Quality Research Division, Environment and Climate Change Canada, 4905 Dufferin Street,
9 Toronto, Ontario, M3H 5T4, Canada

10 ²Air Quality Research Division, Environment and Climate Change Canada, 335 River Road,
11 Ottawa, Ontario, K1V 1C7, Canada

12
13 *Corresponding author:* Craig A. Stroud (craig.stroud@canada.ca)

14
15 **Abstract**

16
17 This study assesses the impact of revised volatile organic compound (VOC) and organic
18 aerosol (OA) emissions estimates in the GEM-MACH (Global Environmental Multiscale–
19 Modelling Air Quality and CHemistry) chemical transport model on air quality model
20 predictions of organic species for the Athabasca oil sands region in Northern Alberta, Canada.
21 The first emissions dataset that was evaluated (base-case run) makes use of regulatory-reported
22 VOC and particulate matter emissions data for the large oil sands mining facilities. The second
23 emissions dataset (sensitivity run) uses total facility emissions and speciation profiles derived
24 from box-flight aircraft observations around specific facilities. Large increases in some VOC and
25 OA emissions in the revised-emissions data set for four large oil sands mining facilities and
26 decreases for others were found to improve the modeled VOC and OA concentration maxima in
27 facility plumes, as shown with the 99th percentile statistic and illustrated by case studies. The
28 results show that the VOC emission speciation profile from each oil sand facility is unique and
29 different from standard petrochemical-refinery emission speciation profiles used for other
30 regions in North America. A significant increase in the correlation coefficient is reported for the
31 long-chain alkane predictions against observations when using the revised emissions based on

32 aircraft observations. For some facilities, larger long chain alkane emissions resulted in higher
33 secondary organic aerosol production, which improved OA predictions in those plumes. Overall,
34 the use of the revised emissions data resulted in an improvement of the model mean OA bias;
35 however, a decrease in OA correlation coefficient and a remaining negative bias suggests the
36 need for further improvements to model OA emissions and formation processes. The weight of
37 evidence suggests that the top-down emission estimation technique helps to better constrain the
38 fugitive organic emissions in the oil sands region, which are a challenge to estimate given the
39 size and complexity of the oil sands operations and the number of steps in the process chain from
40 bitumen extraction to refined oil product. This work shows that top-down emissions estimation
41 technique may help to constrain bottom-up emission inventories in other industrial regions of the
42 world with large sources of VOCs and OA.

43 44 **1 Introduction**

45
46 Chemical transport models (CTMs) are useful tools to support clean energy policy decisions
47 because they can be used to assess the impact of past and future pollutant emission changes on
48 air quality (e.g., Schultz *et al.*, 2003; Kelly *et al.*, 2012; Rouleau *et al.*, 2013; Lelieveld *et al.*,
49 2015). CTMs can also be run in forecast mode with their output being used to support air quality
50 forecasts (Moran *et al.*, 2010; Chai *et al.*, 2013). CTMs require pollutant emission inputs,
51 typically at hourly intervals, at the model grid spatial resolution (Dickson and Oliver, 1991;
52 Houyoux *et al.*, 2003; Pouliot *et al.*, 2012, 2015; Zhang *et al.*, 2017). The pollutant emission
53 input files are based on the processing of emission inventories compiled for all emission sectors,
54 usually at some geopolitical spatial resolution (e.g., county, province/state, or country), and may
55 thus require the application of spatial disaggregation factor fields to allocate emissions to the
56 model grid. North American emission inventories are typically derived from bottom-up

57 approaches, where representative pollutant emission factors (e.g., pollutant mass emission per
58 volume of fuel burned) are multiplied by activity factors (e.g., volume of fuel burned per unit
59 time). In developed countries, industrial facilities are usually required to report estimates of their
60 pollutant emissions to national inventories such as the National Pollutant Release Inventory
61 (NPRI) in Canada ([Government of Canada, Canada Gazette, 2018](#)) and the National Emissions
62 Inventory (NEI) in the United States ([Office of the Federal Register, Protection of Environment,
63 2015](#)). Updates of these inventories occur under a regulatory framework on a regular basis.
64 However, reporting requirements may be limited to aggregated mass emissions on an annual
65 basis (e.g., a total bulk mass of VOC emitted rather than a detailed and observation-based
66 emissions of individual speciated VOCs), with the subsequent use of VOC speciation profiles
67 (splitting factors) to determine the relative contribution of the individual VOCs to the total VOC
68 emissions. Uncertainties in the availability and assignment of appropriate VOC speciation
69 profiles, spatial and temporal allocation factors (Mashayekhi *et al.*, 2016), and/or unaccounted-
70 for emitting activities, result in the need to evaluate the impact of these assumptions through the
71 comparison of CTM predictions with ambient observations.

72 The Athabasca region of northeastern Alberta, Canada has one of the largest reserves of oil
73 sands (OS) in the world. The OS deposits are composed of bitumen, minerals, sand and clay. Oil
74 sand near the surface is mined by open-pit mining techniques. The oil sand is then transported by
75 heavy hauler trucks to crushers, followed by the addition of hot water to make the oil sand flow
76 through pipelines to a bitumen extraction facility. Here, the bitumen is separated from the sand
77 and clay by the use of organic solvents. The product is used either directly, upgraded on-site to
78 crude oil or transported to a remote upgrader facility. Volatile organic compounds from the
79 bitumen have the potential to escape into the atmosphere as fugitive emissions during the

80 mining, extraction, processing, or tailing discharge steps. The complexity and vast size of the oil
81 sands operations make generating pollutant emission input files for CTMs a challenge (Cho *et*
82 *al.*, 2012; ECCC & AEP, 2016).

83 Organic compounds in the atmosphere are oxidized over time and, in the presence of
84 sufficient levels of oxides of nitrogen, are important precursors to ozone formation (Seinfeld and
85 Pandis, 1998). VOCs and semi-volatile organic compounds (SVOCs) are also precursors to
86 secondary organic aerosol (SOA) formation (Griffin *et al.*, 1999; Kanakidou *et al.*, 2005;
87 Robinson *et al.*, 2007; Kroll and Seinfeld, 2008; Slowik *et al.*, 2010; Stroud *et al.*, 2011; Gentner
88 *et al.*, 2017). If the organic compounds have sufficiently low saturation vapor pressures, then
89 upon release into the atmosphere they remain particle-bound and are classified as primary
90 organic aerosol (POA). Many specific organic compounds can also be toxic to human health and
91 require explicit reporting in emission inventories (Stroud *et al.*, 2016).

92 The Joint Oil Sands Monitoring (JOSM) program was developed by the federal government
93 of Canada and the Alberta provincial government with input and consultation from the local
94 indigenous population and industry stakeholder groups to monitor the potential impacts of
95 pollutant emissions. During JOSM, top-down approaches to estimate emissions based on
96 atmospheric observations provided a unique opportunity to compare with bottom-up calculated
97 emissions for the Athabasca OS facilities in Alberta, Canada (Gordon *et al.*, 2015; Li *et al.*,
98 2017). The mass-balance approach that was used is based on using box-shaped aircraft flight
99 patterns around a facility and measuring pollutant concentrations and meteorological variables
100 (wind speed and direction, air density). In this approach, the difference in pollutant mass fluxes
101 entering and leaving the box is used to determine the total facility-wide emission rate, subject to

102 assumptions such as minimal losses due to chemical oxidation between the emissions location
103 and the nearby aircraft observations.

104 Environment and Climate Change Canada (ECCC)'s chemical transport model, GEM-
105 MACH (Global Environmental Multi-scale-Modelling Air quality and CHEmistry) is being used
106 in JOSM to assess the impact of current emissions and future emission changes on local air
107 quality and downwind regional-scale acid deposition (Makar *et al.*, 2018). In this model study,
108 we make use of both regulatory-inventory-based and aircraft-observation-derived emissions data
109 for VOCs and primary particulate emissions for six large OS mining facilities as inputs to GEM-
110 MACH in order to assess the impact of these two different emission data sets on model
111 predictions of VOC concentrations and OA formation.

112 **2 Methods**

113
114 The GEM-MACH model uses the ECCC operational weather forecast model (Global
115 Environmental Multi-scale, GEM) as the core operator for dynamics and microphysical
116 processes (Côté *et al.*, 1998a,b; Girard *et al.*, 2014). GEM-MACH is an “on-line” CTM - the
117 chemistry, vertical diffusion, and pollutant deposition routines exist as a set of subroutines
118 contained and called from within GEM's meteorological physics package (Moran *et al.*, 2010,
119 Makar *et al.*, 2015ab). The gas-phase chemistry scheme is based on the ADOM-II mechanism
120 (Acid Deposition and Oxidant Model, version II), originally developed for continental boundary-
121 layer oxidant formation. The VOC lumped species used in GEM-MACH are described in Stroud
122 *et al.* (2008). The focus here is on evaluating volatile aromatic and alkane species of
123 anthropogenic origin. The aerosol size distribution is described by a 12-bin sectional approach
124 based on the Canadian Aerosol Module (CAM) (Gong *et al.*, 2003; Park *et al.*, 2011). The SOA
125 scheme is based on a two-product fit to smog chamber data using the SOA yield equations

126 derived from gas/particle partitioning theory (Pankow 1994; Griffin *et al.*, 1999; Barsanti *et al.*,
127 2013). In the GEM-MACH model's current SOA formation algorithms, after initial particle
128 formation, the organic compounds in the particle phase are assumed to be converted rapidly to
129 non-volatile mass, as observed by recent studies (Cappa and Jimenez, 2010; Cappa *et al.*, 2011;
130 Lopez-Hilfiker *et al.*, 2016) and recommended by modelling studies (Shrivastava *et al.*, 2015).
131 However, other recent observation studies suggest that SOA 'chemical aging' over hours to days
132 is quite complex, and involves further gas-phase oxidation and fragmentation reactions (Jimenez
133 *et al.*, 2009; Donahue *et al.*, 2014), as well as potential particle-phase oxidation and oligomer
134 reactions (McNeill *et al.*, 2015). The particle oligomer reactions are rapid, often acid-catalyzed,
135 and can result in conversion to non-volatile mass (Liggio *et al.*, 2005; Kroll *et al.*, 2005). We
136 discuss below the evidence from this work on the likelihood that these additional missing
137 processes are still impacting our model organic aerosol bias.

138 2.1 Emissions

139 The Canadian base-case emissions were derived by combining several emission inventories,
140 targeting 2013 as the base year. This base year was chosen to align with the JOSM 2013
141 intensive field study period, which provided the observations for the model/observation
142 comparisons that follow. Canadian emissions for industrial facilities, including the Athabasca OS
143 mining facilities, were obtained from the 2013 NPRI. The U.S. base-case emissions were
144 obtained from the 2011 U.S. NEI Version 1 (Eyth *et al.*, 2013).

145 These base-case, bottom-up emissions inventories were processed with the SMOKE (Sparse
146 Matrix Operator Kernel Emissions) emissions processing tool
147 (<https://www.cmascenter.org/smoke>), which includes three major steps corresponding to spatial
148 allocation, temporal allocation, and chemical speciation (for NO_x, VOC, and PM). The base-case

149 VOC speciation profiles used by SMOKE for the OS surface mining facilities were obtained
150 from the CEMA (Cumulative Environmental Management Association) inventory (Davies *et al.*,
151 2012; Zhang *et al.*, 2015).

152 For the sensitivity run, speciated VOC emissions from the base case for four OS mining
153 facilities (Suncor Millenium/Steepbank, Syncrude Mildred Lake, Shell Canada
154 Muskeg/Jackpine, and CNRL Horizon) were revised by replacing them with the top-down
155 emission rates estimated by Li *et al.* (2017) while primary PM emissions were revised for six oil
156 sand facilities (Suncor Millenium/Steepbank, Syncrude Mildred Lake, Shell Canada
157 Muskeg/Jackpine, CNRL Horizon, Syncrude Aurora North, and Imperial Oil Kearn) (Zhang *et*
158 *al.*, 2018). The VOC and PM chemical speciation profiles used for these facilities were also
159 revised using the aircraft-observed VOC speciation (Li *et al.*, 2017) and ground-based PM filter
160 analysis (Wang *et al.*, 2015), respectively. The set of emissions input files making use of these
161 revisions is hereafter referred to as the “revised emissions”, while the original emissions input
162 files without these changes is referred to as the “base-case emissions”. A detailed description of
163 the development of the emission inventory and emissions processing steps to create the model-
164 ready files (hourly gridded emission fields for the same domain and grid spacing as the model)
165 for the base case and revised version are described in Zhang *et al.* (2018). Table 1 compares the
166 facility emission rates for four species for the base case and revised-emissions case. The changes
167 are not consistent from species to species and are not uniform across facilities. Interestingly, the
168 facilities that use paraffinic solvents for bitumen extraction (e.g. Shell Muskeg/Jackpine) were
169 associated with the largest ALKA emission (long chain alkanes) increases and aromatic
170 decreases. The SI section includes figures illustrating the emission difference maps for the oil
171 sand region (absolute and relative difference) showing the spatial distribution of emission

172 changes between revised and base case. The changes are largest over the surface mines and
173 tailing ponds.

174 Depending on whether bitumen extracted from the oil sand is upgraded on site or not, the OS
175 mining facilities can be classified into two broad types: (1) integrated extraction and upgrading
176 facilities (Suncor Millenium/Steepbank, Syncrude Mildred Lake, and CNRL Horizon) and (2)
177 extraction-only facilities (Shell Canada Muskeg/Jackpine, Syncrude Aurora North, and Imperial
178 Oil Kearn). Table 2 shows a comparison of the CEMA plant-specific VOC speciation profiles
179 used in the base case for the two types of OS plants compared to two standard VOC speciation
180 profiles for petrochemical facilities (#9012 “Petroleum Industry – Average”, #0316 “Fugitive
181 Emissions, Pipe/Valve Flanges”) that were used by SMOKE to speciate more than half of the
182 refinery emissions in the Houston area, the largest petrochemical cluster in the U.S. There are
183 significant differences between the base case OS plant VOC speciation profiles and the two
184 commonly used standard oil refinery profiles. The OS integrated extraction and upgrading plant
185 profiles are higher in long-chain alkenes, toluene, and other aromatics than the standard profiles,
186 while the extraction-only plant profile has the highest long-chain alkane fraction. The two
187 standard profiles used for the base case and revised simulation (for speciating U.S. and Canadian
188 refinery emissions) have higher less-reactive species (e.g., propane, acetylene) and formaldehyde
189 (profile #9012), than both the CEMA OS plant profiles. Note also that these differences in
190 relative fractions result in substantial differences in the absolute emissions of certain groups of
191 VOCs between the standard profiles for oil refineries and the facility-specific oil sand profiles.
192 For reference, the aircraft-measurement-derived facility-specific VOC speciation profiles used
193 for four OS facilities in the revised-emissions case are presented in Zhang *et al.* (2018). The
194 aircraft-measurement-derived profiles in Zhang *et al.* (2018), and used here for the revised case,

195 are composite profiles since they encompass plant, tailing pond and mining emissions. As such,
196 they are not appropriate for comparison with the profiles in Table 2, which are specific to plant
197 emissions.

198 The primary PM emissions from the OS facilities originate largely from off-road heavy-duty
199 diesel trucks, plant stack emissions, and fugitive and wind-blown dust. The 2009/10 CEMA
200 inventory was used to specify the tail-pipe emissions from the off-road mining fleet and the 2013
201 NPRI inventory was used for fugitive road-dust emissions. The base-case inventory did not
202 include wind-blown dust. For the revised inventory, the PM size distribution was measured
203 during the 2013 field study for all six facilities and these data were used to constrain the revised
204 PM emission input data set. Note that the PM emissions estimates based on the aircraft-measured
205 aerosol data included the contribution of wind-blown dust emissions. The aircraft-based PM
206 emissions were re-binned for the 12 GEM-MACH PM size bins. The first eight size bins
207 correspond to mass up to diameter 2.56 μm . Interestingly, the aircraft measured a much higher
208 fraction of particulate mass in bin 8 (bounded by diameters 1.28 and 2.56 μm) compared to the
209 mass fraction in bin 8 from the area-source PM size-distribution profiles used by SMOKE in
210 processing the base-case emissions. In addition, a PM chemical speciation profile specific to OS
211 fugitive dust emissions was created from an analysis of deposited dust collected from surfaces in
212 the OS region (Wang *et al.*, 2015); this speciation profile replaced the standard fugitive dust
213 profile for unpaved roads from the U.S. EPA (Environmental Protection Agency) SPECIATE
214 v4.3 database in the revised emissions processing. The resulting organic carbon fraction in the
215 observation-derived PM speciation profile was higher than that of the base-case emissions by
216 about a factor of 3 (Zhang *et al.*, 2018). In general, significantly higher POA emissions were

217 observed over the open-pit mines for all facilities, except for the Imperial Kearn mine. The
218 impact of the revised POA emissions will be discussed further in Section 3.4.

219 2.2 Modeling

220 The GEM-MACH model was run in a nested configuration with an outer domain covering the
221 continental U.S. and Canada and an inner domain covering Alberta and Saskatchewan. The
222 continental-scale GEM-MACH model (10-km resolution) and the Canada-wide GEM weather
223 model (2.5-km resolution) were run first. These provided the chemical and meteorological lateral
224 boundary conditions, respectively, for the high-resolution GEM-MACH 2.5-km resolution run,
225 which has a domain covering the provinces of Alberta and Saskatchewan (Figure 1). The two
226 models providing boundary conditions were run on a 30-hour cycle, of which the first six hours
227 were spin-up and discarded, while the remaining 24 hours provided boundary conditions for the
228 2.5-km GEM-MACH simulation. The initial conditions subsequent to the starting model
229 simulation for each overlapping 24-hour 2.5-km GEM-MACH simulation came from the end of
230 the previous 2.5-km GEM-MACH simulation. This strategy was used to allow the two boundary
231 condition simulations to make use of assimilated meteorological analyses. The sequence of
232 model simulations was started for August 10, 2013 and run until September 7 to cover the 2013
233 JOSM intensive field study period.

234 2.3 Observations

235 The NRC (National Research Council) Convair two-engine turboprop aircraft was used to
236 collect air-quality observations during the JOSM 2013 intensive field study. The aircraft was
237 equipped with a suite of instruments to measure air quality over 22 flights (see Li *et al.*, 2017,
238 Figure S1). Most of the flight hours focused on “box” flight paths; these took the aircraft around
239 the periphery of facilities at different heights, with the goal of deriving facility-wide emission

240 rates by using observations of chemical concentrations and winds to estimate the mass of
241 pollutants entering and leaving the box enclosures. Coupled with a mass-conserving flux model
242 (Gordon *et al.*, 2015), these aircraft data were used to estimate emissions from the encircled
243 facilities.

244 VOC and PM observations were collected by the instrumented research aircraft using
245 different technologies. A proton-transfer-reaction mass spectrometer (PTR-MS) was used to
246 measure a select number of VOCs at high temporal resolution (1-sec) (Li *et al.*, 2017). An
247 aerosol mass spectrometer (AMS) was used to measure PM₁ mass and non-refractory chemical
248 composition (Liggio *et al.*, 2016). A Single Particle Soot Photometer (SP2) was used to measure
249 refractory black carbon aerosol (Liggio *et al.*, 2016). A number of canisters were filled with
250 ambient air on each flight and returned to the lab for GC-FID (Gas Chromatograph with Flame
251 Ionization Detector) and GC-MS (Gas Chromatograph with Mass Spectrometer) analysis of
252 VOCs (Li *et al.*, 2017). The canister VOC analysis measured 154 different C₂ to C₁₂
253 hydrocarbons (Dann and Wang, 1995). The resulting observation data were compared to the
254 model output generated as described above. The 2.5-km GEM-MACH runs used a 120-s
255 chemistry time step; 120-s model output values were linearly interpolated in time and space to
256 the aircraft observation locations; all comparisons which follow make use of the resulting
257 model/observation data pairs for the two simulations.

258 **3 Results and Discussion**

259 We present our evaluation results for four species classes: mono-substituted aromatics in
260 section 3.1; multi-substituted aromatics in section 3.2; long-chain alkane species in section 3.3;
261 and organic aerosols in section 3.4.

263 **3.1 Toluene and other Mono-Substituted Aromatics (TOLU) Evaluation**

264

265 The aircraft PTR-MS measurement data set was averaged to 10-sec intervals for comparison
266 to the GEM-MACH model output. The model grid cell output was extracted along the flight
267 track and interpolated linearly between the two minute model output intervals to create a
268 coincident model and measurement time series. The model lumped TOLU species includes
269 toluene and other mono-substituted aromatics with the two most important additional species
270 being ethyl-benzene and propyl-benzene. Therefore, we must derive an equivalent observed
271 lumped TOLU species for a comparison. We used all of the canister VOC data from the field
272 study to create ethyl-benzene vs. toluene and propyl-benzene vs. toluene scatterplots. The
273 corresponding slope, y-intercept and correlation coefficient for both these plots (not shown) were
274 as follows: $m=0.376\pm 0.006$, $y=0.0328\pm 0.006$, $R=0.91$ and $m=0.0652\pm 0.0008$, y -
275 $intercept=0.0011\pm 0.0008$, $R=0.90$, respectively. Thus, we derived an observed TOLU equal to
276 the PTR-MS C7 aromatic multiplied by the factor 1.4412 (sum of $m=1.0 C7+0.376 C7+0.0652$
277 $C7$). This new observation-derived TOLU was used in the statistical comparison with model
278 output TOLU, which follows.

279 Histograms of mixing ratio were created using the observed TOLU, the revised-emissions
280 model output, and the base-case model output. Figure 2 illustrates the histograms using 20
281 mixing-ratio bins and an increment of 0.2 ppbv per bin. It is clear that there are more high values
282 (>2 ppbv) produced by the sensitivity model run with revised emissions compared to the base-
283 case model run. The number of observations in the highest value bins lies between the results
284 from the revised and base-case versions. This can be quantified by using the 99% percentile
285 statistic (obs=1.258 ppbv, revised=1.906 ppbv, base=0.934 ppbv). The 99% percentile means
286 that 99% of the data points are lower than the value. The median concentration of the
287 observations (0.061 ppbv) is higher than both the revised (0.038 ppbv) and base-case model

288 (0.019 ppbv) simulated values, but is closer to the revised version. Table 3 lists statistical scores
289 for the TOLU lumped species and the other species considered in this study. The mean bias goes
290 from a negative value with the base-case run to a positive value with the revised emissions.
291 There is little difference in the correlation coefficient for the model vs. observation scatterplot
292 between the base-case and sensitivity run. The changes to the VOC emissions for the revised-
293 emissions run affected their total mass and speciation, and the observations were made
294 sufficiently close to the sources that there was little time for oxidation. The main sources for
295 VOCs are the processing plants, tailing ponds, mine faces, and off-road vehicles and their spatial
296 allocation (from CEMA, 2010) did not change significantly between the two model-emission
297 versions. The main differences in the model time series between the two simulations are thus in
298 magnitude of concentrations, and hence relatively invariant correlation coefficients might be
299 expected. The correlation coefficient is more likely controlled by the meteorological model
300 accuracy in the placement of the plumes (i.e. wind direction).

301 The largest increases in the TOLU emission, between the revised and base case run, are noted
302 for the Syncrude Mildred Lake facility over the tailing ponds and open pit mine faces. Table 1
303 shows the changes on a facility-wide level. Notable increases are also calculated for the Suncor
304 Millennium/Steepbank and the Canadian Natural Resources Ltd (CNRL) Horizon facilities. The
305 flights on August 14 and 23 have the largest TOLU mixing ratios for the aircraft study, and both
306 flights correspond to box flights around the Syncrude Mildred Lake facility. The SI section
307 includes the model and measurement time series comparisons (termed case studies) for the
308 flights on August 14 (Figure S5) and August 23 (Figure S6). Overall, the magnitude of the
309 mixing ratio maximum in the time series are better represented in the revised-emission

310 simulation. This is also reflected in the better slope statistic in Table 3 for the revised-emission
311 simulation.

312 **3.2 Multi-Substituted Aromatics (AROM) Evaluation**

313
314 The model lumped AROM species includes all multi-substituted aromatics, with the most
315 important species being the xylene isomers and trimethylbenzene isomers. These two species
316 match with the PTR-MS C8 and C9 aromatic fragments, respectively. However, the observed C8
317 aromatic also includes ethyl-benzene and the C9 aromatic also includes propyl-benzene, which
318 are lumped with TOLU in the model VOC speciation. Thus, we need to subtract these unwanted
319 species from the totals used to compare to the model lumped AROM species. To do this, we use
320 their correlation slopes with PTR-MS C7 aromatic from Section 3.1. The new observation-
321 derived AROM was calculated from the PTR-MS measurements as follows: $C8 + C9 - 0.376 C7$
322 $- 0.0652 C7$.

323 Figure 3 shows the histograms for the lumped AROM species for 10-sec averaged points
324 along all the flight tracks. The base model has a large number of high value points (> 2 ppbv),
325 many more than the model simulations with the revised emissions, and also more than the
326 observations. This can be quantified by using the 99% percentile (obs=0.7607, revised=1.004,
327 base case=2.302). The median value for the observations is 0.0182 ppbv, smaller than both the
328 model versions (revised=0.0236 ppbv, base case=0.0466 ppbv), but closer to the model driven by
329 the revised emissions. Table 3 lists other statistical scores for the AROM lumped species. The
330 mean bias and RMSE (root mean square error) are smaller for the revised emissions run
331 compared to the base case. However, there is a small degradation in the correlation coefficient
332 with the sensitivity run.

333 The largest decreases in the AROM emission field between the revised and base case
334 emissions are again over the Syncrude Mildred Lake facility (refer to Table 1). There were also
335 notable decreases over the CNRL Horizon and Shell Muskeg/Jackpine facilities, but positive
336 changes in AROM emissions were noted over the Suncor Millennium/Steepbank facility (also
337 refer to Figure S2 for the emission spatial difference map). The SI section includes the model
338 and measurement time series comparison for the flights on August 23 and September 3. In
339 general, the observed mixing ratio changes are closer in magnitude to the predictions from the
340 revised-emission simulation compared to the base case for the plume intersects.

341 **3.3 Long-Chain Alkanes (ALKA) Evaluation**

342 The long-chain alkanes (C_4 to C_{12}) were sampled by filling canisters with ambient air on-
343 board the aircraft. Figure 4 presents the histogram for the long-chain alkanes. The mixing ratios
344 are divided into 20 bins each with a width of 3 ppbv. From the observed histogram, there is a
345 wide range to the mixing ratios with a small number of very large concentrations, but also the
346 first bin (0 to 3 ppbv) has a high percentage of the points. The model gas-phase mechanism
347 represents all higher carbon-number alkanes by a single lumped species, with chemical and
348 physical properties derived from C_4 to C_8 alkanes. The base-case run calculates lower ALKA
349 mixing ratios than the model version using revised emissions. The model using revised emissions
350 is much better at reproducing the higher concentration points, particularly above 12 ppbv. This is
351 quantified by the 99% percentile of the data sets (obs=29.9, base=18.0 revised=24.6). Other
352 statistics for the lumped ALKA species are shown in Table 3. The mean bias went from a small
353 negative value to +1.98 ppbv. The slope decreased by a small value, but the y-intercept
354 increased, which also increased the RMSE for the run with the revised emissions. The correlation
355 coefficient improved significantly for the model run with revised emissions.
356

357 The revised ALKA emissions are considerably higher for the CNRL Horizon and Shell
358 Muskeg/Jackpine facilities, but have smaller changes for the other facilities (refer to Table 1),
359 possibly reflecting differences in the processing activities between the facilities. Overall, the time
360 series analysis for the aircraft flights (refer to Figures S10 and related discussion in SI) showed
361 mixed improvements for ALKA associated with the revised emissions. The large increases in
362 ALKA emissions in the sensitivity simulation for the CNRL facility did improve the model
363 maxima for the plume intersects on August 26. The analysis suggests further improvement in
364 spatial allocation for the Shell facility may be needed. The higher ALKA mixing ratios also feeds
365 back to higher SOA formation downwind of these facilities, as discussed below.

366 The use of aircraft observations to both derive emissions data and evaluate the subsequent
367 model simulations might be taken as circular reasoning. We note first that observation-derived
368 emissions are frequently used in modelling (for example, Continuous Emissions Monitoring
369 System concentration observations are used to generate emissions data for large stack emitters),
370 and second, that the emissions are only one component of the overall modelling system. An
371 improvement in the simulated VOC concentrations using observation-based emissions is only
372 guaranteed if the emissions dominate the net model error. While our results show that, in general,
373 the new emissions information does improve model performance, the results using that new data
374 are not perfect, indicating other sources of error are contributing to the overall model
375 performance.

376 **3.4.1 Organic Aerosol (OA) Evaluation**

377 Figure 5 illustrates the histograms for the organic aerosol observations and model results
378 with base case and revised emissions. A clear improvement is shown in the highest concentration
379 bins ($>15 \mu\text{g}/\text{m}^3$) with the revised emissions. This can be quantified with the 99th percentile of

380 the data (obs=13.4 $\mu\text{g}/\text{m}^3$, revised=9.3 $\mu\text{g}/\text{m}^3$, base=4.9 $\mu\text{g}/\text{m}^3$). The median statistic also
381 improved (obs=2.8 $\mu\text{g}/\text{m}^3$, revised=0.84 $\mu\text{g}/\text{m}^3$, base=0.70 $\mu\text{g}/\text{m}^3$). The lower 5th percentile is
382 also significantly under-predicted compared to observations and does not change much between
383 the two model runs (obs=0.49 $\mu\text{g}/\text{m}^3$, revised=0.036 $\mu\text{g}/\text{m}^3$, base=0.035 $\mu\text{g}/\text{m}^3$). This reflects an
384 under-prediction in the background OA predicted by the model, which is likely due to low
385 biogenic SOA formation and aging in both model versions. The importance of widespread
386 biogenic SOA formation from boreal forests has been reported in other work (Slowik *et al.*,
387 2010; Tunved *et al.*, 2006).

388 Additional statistics are presented in Table 3. The mean bias, RMSE and slope all improve for
389 the revised-emissions run, though the correlation coefficient decreases significantly for this run.
390 To investigate the variability in the OA bias, we plotted the OA bias as a function of different
391 measured variables. Figure 6 is a plot of the OA bias as a function of the observed black carbon
392 (BC) aerosol for the base-case and sensitivity runs. The BC is a marker for petrochemical
393 combustion, particularly diesel. For the base-case run, the OA negative bias is observed to
394 increase in magnitude with observed BC. Points with high observed BC correlate well with
395 emissions from the OS open-pit mines (Liggio *et al.*, 2017), where the BC is likely emitted from
396 the heavy-hauler trucks. The locations with the largest OA bias were also consistent with the
397 locations of mines and the transport wind direction. A review of the OS emission inventories
398 suggest that about 70% of the BC comes from the OS off-road diesel fleet. Including all points,
399 the mean bias improves from -2.8 to -2.4 (see Table 3) when using the revised emissions. Figure
400 6b shows a zoomed plot for points with high observed BC ($>0.8 \mu\text{g}/\text{m}^3$). There is a clear
401 improvement in bias for most of these points. The average bias for these high BC points
402 improves from -6.8 $\mu\text{g}/\text{m}^3$ for the base case to -2.6 $\mu\text{g}/\text{m}^3$ for the revised emissions. For

403 emissions processing the increase in PM emissions was assigned to the processing plants
404 (particle bin diameter $D < 1 \mu\text{m}$) or the surface mines (particle bin diameter $D > 1 \mu\text{m}$). Overall,
405 Figure 6 shows that, while the negative OA bias improves for samples high in BC concentration
406 (i.e. influenced by petrochemical combustion or collocated with petrochemical combustion
407 sources), there still remains an unaccounted for negative OA bias.

408 Figure 7 is a scatterplot of the difference in predicted POA between the revised and base-case
409 emissions runs vs. the difference in predicted total OA. A large fraction of the points fall along
410 the 1:1 line, and hence for these points the difference between the two runs is almost completely
411 due to the increased total primary PM emissions, and increased POA fraction of those emissions,
412 of the revised emissions simulations. The points with largest concentrations along the 1:1 line
413 correspond to flights over the Syncrude Mildred Lake facility on Aug. 16, Aug. 23 and Sept. 3.
414 There is a subset of points, however, that lies below the 1:1 line; these correspond to points with
415 significantly enhanced model SOA between the two runs (Aug. 16 flight over CNRL Horizon
416 and Aug. 21 survey flight over Shell Muskeg/Jackpine). The SI section includes the model and
417 measurement time series comparisons for the flights on August 21, August 23 and September 3.
418 Overall, the case studies showed improved predictions for the magnitude of the organic aerosol
419 change for the plume passages with the revised emissions; however, the base line organic aerosol
420 was over-predicted for all case studies.

421 **3.4.2 Organic Aerosol Model Recommendations**

422 The improvement in model PM_{10} OA bias due to the use of the revised emissions is
423 encouraging; however, the decrease in correlation coefficient suggests that the spatial allocation
424 of PM_{10} emissions may need further refinement. The remaining negative bias suggests that other

425 important processes may be missing or under-represented in the model. Three recommendations
426 emerge from recent and current work:

427 1) SOA Formation from Fugitive IVOC Emissions

428 Recent publications suggest that fugitive intermediate volatile organic (IVOC) emissions
429 from the OS open-pit mines are needed to represent SOA formation downwind of the OS region
430 (Liggio *et al.*, 2016). In our emissions revision, only a small portion of the IVOCs (dodecane
431 C₁₂) were added and lumped into the long-chain ALKA lumped species. IVOC species with
432 carbon number ≥ 13 were not measured by the Li *et al.*, (2017) aircraft study and thus we do not
433 have revised IVOC emissions included in this work. Furthermore, the ALKA lumped species has
434 an SOA yield more representative of a lower molecular-weight range, and the yield is known to
435 increase with increasing carbon number, so the dodecane SOA contribution would be
436 underestimated. Work is currently underway with GEM-MACH to implement a Volatility Basis
437 Set (VBS) approach to SOA formation. The VBS approach will more adequately represent the
438 intermediate and semi-volatile volatility range and chemical aging of this lower volatility
439 compounds (Robinson *et al.*, 2006). Future work will measure IVOC emissions using box flights
440 around the oil sand facilities and open-pit mines. This will remove current uncertainties in
441 models and help improve the negative bias in plumes. Implementing the VBS scheme will also
442 enable the PM emissions used here (in both data sets) to be distributed into volatility bins.

443 Also, while the measurement-derived emissions are missing the IVOCs, the measurement-
444 derived POA emissions may contain some gaseous VOCs, IVOCs and SVOC species that react
445 quickly and in one oxidation step yield products that condense onto particles. This rapid SOA
446 mass produced would be measured in the box flights and, at least partially, accounted for in the
447 updated OA emissions; however labeled here as POA instead of fresh SOA. Furthermore, there

448 is the potential for double counting if some of the very reactive gaseous precursors react to form
449 SOA and this is accounted for in the measured POA. In this paper, we have tried to minimize this
450 effect by examining the model performance in the “near field” from emission flights close to
451 facilities. This will be the topic of future box modelling work with the new 2018 measurement-
452 derived IVOC and SVOC emissions to determine how much of the measurement-derived POA is
453 derived from the fugitive open-pit mining IVOC and SVOC emissions and their rapid particle
454 formation.

455 2) Background Organic Aerosol Levels

456 The under-prediction in background OA was a general finding from the study; the cause is
457 believed to be due to underestimated biogenic SOA, due to the lumping of biogenic monoterpene
458 emissions into the anthropogenic ALKE model species in the model’s gas-phase mechanism, and
459 the lack of speciated representation of other biogenic SOA precursors such as sesquiterpenes.
460 Future work will update the biogenic SOA yield coefficients in the VBS approach using recent
461 smog chamber results which account for gas-phase loss of organic species to chamber walls (Ma
462 *et al.*, 2017).

463 3) Spatial Allocation of Emissions

464 Future field studies should also focus on improving within-facility spatial allocation. For
465 example, within-facility data such as the GPS (Global Positioning System) location of the mining
466 trucks would be helpful to derive their activity diurnal profiles and to improve truck emission
467 spatial allocation within a facility. The GPS data would also be useful to define the location of
468 freshly excavated open-pit mines within a facility.

469 **4 Conclusions**

470

471 Overall, the weight of evidence suggests that the top-down emission estimation technique
472 applied to the OS surface mining facilities helps to better constrain reported facility-total organic
473 emissions including fugitive sources, as shown by improved model results when the revised
474 emissions are employed. We note that emissions from these sources are a challenge to calculate
475 in bottom-up inventories due to the potential for fugitive emissions. For the mono- and multi-
476 substituted aromatics (TOLU and AROM), the emission rates from facilities were more fine
477 adjustments, as some facility totals went up and some went down and the overall biases
478 compared to observations improved for AROM but degraded for TOLU. However, the model's
479 ability to predict very high aromatic concentrations in plumes improved with the revised
480 emissions, as shown by the 99th percentile statistic and the case studies.

481 For the long-chain ALKA species, the revised emissions may have over-corrected, on
482 average, as shown by the increase in mean bias for the entire aircraft data set. However, the
483 correlation coefficient did improve significantly for the long-chain alkane predictions, suggesting
484 the combination of alkane emission increases for some facilities and decreases for others helped
485 to improve the spatial distribution of ALKA emissions. The results for some facilities suggest
486 that further improvement could be achieved by putting more emissions at extraction processing
487 plant locations (i.e., adjusting within-facility spatial allocation). Interestingly, the alkane
488 emission increases and aromatic emission decreases, derived from aircraft data (Li *et al.*, 2018),
489 were associated with the facilities that use paraffinic solvents for bitumen extraction (e.g. Shell
490 Muskeg/Jackpine). Overall, the predictions of alkanes in high concentration plumes improved
491 with the revised emission data set, as shown by the 99th percentile statistic.

492 For PM₁ organic aerosol, the revised emissions improved the mean bias for predictions;
493 however, a negative bias still exists and the improvement was associated with a decrease in

494 correlation coefficient. The increase in predicted PM₁ OA concentration was largely due to the
495 increase in POA emissions in the revised emissions input files. The POA emissions increased
496 because of a combination of larger measurement-derived PM₁ emissions and the revised ground-
497 observed PM speciation profile having a larger POA fraction. The increase in PM₁ POA
498 emissions were largely allocated spatially to stack locations and this allocation may be a key
499 factor in the degradation of the correlation coefficient, especially if the fine OA originates from
500 mine-face fugitive emissions. Future work should focus on improving within-facility spatial
501 allocation of emissions. The remaining negative bias in plumes likely stems from missing IVOC
502 emissions in both the emission data sets used here, as suggested by Liggió *et al.* (2015). Ongoing
503 field work to measure the IVOC emissions using aircraft box flights is underway in a new 2018
504 measurement intensive. Upcoming modelling work with GEM-MACH will include the VBS
505 approach to better represent lower volatility compounds.

506 **Acknowledgements**

507
508 The authors are grateful to all of the participants in the 2013 JOSM intensive field study for their
509 commitment. The authors are also appreciative of the ECCC Pollutant Inventory and Reporting
510 Division (PIRD) and the U.S. EPA for developing, maintaining, and distributing each country's
511 national emission inventories. We also appreciate the efforts of George Marson of ECCC in
512 helping to compile the various emissions inventories from Alberta Environment and Parks, and
513 also CEMA. We also appreciate the analysis of the NAPS VOC measurement group. This study
514 was funded by the Joint Oil Sands Monitoring program and the Climate Change and Air Quality
515 Program.

516 **References**

517
518 Akingunola, A., Makar, P.A., Zhang, J., Darlington, A., Li, S.M., Gordon, M., Moran, M.D., and Zheng, Q.,
519 Evaluation of GEM-MACH Air Quality Modelling at 2.5km Resolution Using JOSM 2013 Intensive Campaign:
520 Impact of Continuous Monitoring Emissions Stack Parameters on Model Simulations, accepted in ACP, 2018.

521
522 Barsanti, K.C., Carlton, A.G., and Chung, S.H., Analyzing experimental data and model parameters: Implications
523 for predictions of SOA using chemical transport models, *Atmos. Chem. and Phys.*, 13 (23), 12073-12088, **2013**.
524
525 Cappa, C.D. and Jimenez, J., Quantitative estimates of the volatility of ambient organic aerosol, *Atmos. Chem.*
526 *Phys.*, 10 (12), 5409-5424, **2010**.
527
528 Cappa, C.D. and Wilson, K.R., Evolution of organic aerosol mass spectra upon heating: Implications for OA phase
529 and partitioning behavior, *Atmos. Chem. and Phys.*, 11 (5), 1895-1911, **2011**.
530
531 Chai, T., Kim, H.-C., Lee, P., Tong, D., Pan, L., Tang, Y., Huang, J., McQueen, J., Tsidulko, M., and Stajner, I.,
532 Evaluation of the United States National Air Quality Forecast Capability experimental real-time predictions in 2010
533 using Air Quality System ozone and NO₂ measurements, *Geoscientific Model Development*, 6 (5), 1831-1850,
534 **2013**.
535
536 Cho, S., McEachern, P., Morris, R., Shah, T., Johnson, J., and Nopmongcol, U., Emission sources sensitivity study
537 for ground-level ozone and PM 2.5 due to oil sands development using air quality modeling system: Part I- model
538 evaluation for current year base case simulation, *Atmos. Environ.*, 55, 533-541, **2012**.
539
540 Cohan, D.S. and Napelenok, S.L., Air Quality Response Modeling for Decision Support, *Atmosphere*, 2, 407-425,
541 **2011**.
542
543 Côté, J., Gravel, S., Méthot, A., Patoine, A., Roch, M., and Staniforth, A., The operational CMC/MRB global
544 environmental multiscale (GEM) model. Part 1: design considerations and formulation, *Mon. Wea. Rev.*, 126, 1373-
545 1395, **1998**.
546
547 Côté, J., Desmarais, J.-G., Gravel, S., Méthot, A., Patoine, A., Roch, M., and Staniforth, A., The operational CMC-
548 MRB global environment multiscale (GEM) model. Part II: results, *Mon. Wea. Rev.*, 126, 1397-1418, **1998**.
549
550 Dann, T.F., Wang, D.K., Ambient air benzene concentrations in Canada (1989-1993): Seasonal and day of week
551 variations, trends, and source influences, *Journal of the Air and Waste Management Association*, 45 (9), pp. 695-
552 702, **1995**.
553
554 Davies, M., Person, R., Nopmongcol, U., Shah T., Vijayaraghavan, K., Morris, R., and Picard, D., Lower Athabasca
555 Region Source and Emission Inventory, report prepared by Stantec Consulting Ltd. and ENVIRON International
556 Corporation for Cumulative Environmental Management Association - Air Working Group,
557 [http://library.cemaonline.ca/ckan/dataset/0cfaa447-410a-4339-b51f-e64871390efe/resource/fba8a3b0-72df-45ed-
558 bf12-8ca254fdd5b1/download/larsourceandemissionsinventory.pdf](http://library.cemaonline.ca/ckan/dataset/0cfaa447-410a-4339-b51f-e64871390efe/resource/fba8a3b0-72df-45ed-bf12-8ca254fdd5b1/download/larsourceandemissionsinventory.pdf), 274 pp., **2012** (last accessed on October 24,
559 2017).
560
561 Dickson, R.J. and Oliver, W.R., Emissions models for regional air quality studies, *Environ. Sci. Technol.*, 25, 1533-
562 1535, **1991**.
563
564 Donahue, N.M., Robinson, A.L., Trump, E.R., Riipinen, I., and Kroll, J.H., Volatility and aging of atmospheric
565 organic aerosol, *Topics in Current Chemistry*, 339, 97-144, **2014**.
566
567 Environment and Climate Change Canada & Alberta Environment and Parks: Joint Oil Sands Monitoring Program
568 Emissions Inventory Compilation Report, [http://aep.alberta.ca/air/reports-data/documents/JOSM-
569 EmissionsInventoryReport-Jun2016.pdf](http://aep.alberta.ca/air/reports-data/documents/JOSM-EmissionsInventoryReport-Jun2016.pdf), 146 pp, **2016**.
570
571 Eyth, A., Mason, R., and Zubrow, A.: Development and Status of EPA's 2011 Modeling Platform, 12th CMAS
572 Conference, 28-30 Oct., Chapel Hill, North Carolina,
573 https://www.cmascenter.org/conference//2013/slides/eyth_development_status_2013.pptx, **2013**.
574
575 Gentner, D.R., Jathar, S.H., Gordon, T.D., Bahreini, R., Day, D.A., El Haddad, I., Hayes, P.L., Pieber, S.M., Platt,
576 S.M., De Gouw, J., Goldstein, A.H., Harley, R.A., Jimenez, J.L., Prévôt, A.S.H., and Robinson, A.L., Review of

577 Urban Secondary Organic Aerosol Formation from Gasoline and Diesel Motor Vehicle Emissions, *Environ. Sci.*
578 *Technol.*, 51 (3), 1074-1093, **2017**.
579

580 Girard, C., Plante, A., Desgagné, M., McTaggart-Cowan, R., Côté, J., Charron, M., Gravel, S., Lee, V., Patoine, A.,
581 Qaddouri, A., Roch, M., Spacek, L., Tanguay, M., Vaillancourt, P.A., and Zadra, A., Staggered vertical
582 discretization of the Canadian environmental multiscale (GEM) model using a coordinate of the log-hydrostatic-
583 pressure type, *Monthly Weather Review*, 142, 1183-1196, **2014**.
584

585 Gong, S.L., Barrie, L.A., Blanchet, J.-P., von Salzen, K., Lohmann, U., Lesins, G., Spacek, L., Zhang, L.M., Girard,
586 E., Lin, H., Leaitch, R., Leighton, H., Chylek, P., and Huang, P., Canadian Aerosol Module: A size-segregated
587 simulation of atmospheric aerosol processes for climate and air quality models 1. Module development, *J. Geophys.*
588 *Res. Atmos.*, 108, **2003**.
589

590 Gordon, M., Li, S.-M., Staebler, R., Darlington, A., Hayden, K., O'Brien, J., and Wolde, M., Determining air
591 pollutant emission rates based on mass balance using airborne measurement data over the Alberta oil sands
592 operations. *Atmos. Meas. Tech.*, 8, 3745-3765. doi:10.5194/amt-8-3745-2015, **2015**.
593

594 Government of Canada, Notice with respect to the substances in the National Pollutant Release Inventory for 2018
595 and 2019, *Canada Gazette Part I*, Vol. 152, No. 3, pp. 129-172, ISSN 1494-6076, Ottawa, January 20, **2018**.
596

597 Griffin, R.J., Cocker III, D.R., Flagan, R.C., and Seinfeld, J.H., Organic aerosol formation from the oxidation of
598 biogenic hydrocarbons, *J. Geophys. Res. Atmos.*, 104 (D3), 3555-3567, **1999**.
599

600 Houyoux, M.R., Vukovich, J.M., Coats, Jr., C.J., Wheeler, N.J.M., and Kasibhatla, P.S., Emission inventory
601 development and processing for the Seasonal Model for Regional Air Quality (SMRAQ) project, *J. Geophys. Res.*,
602 105, 9079-9090, **2000**.
603

604 Jimenez, J.L., Canagaratna, M.R., Donahue, N.M., Prevot, A.S.H., Zhang, Q., Kroll, J.H., DeCarlo, P.F., Allan, J.D.,
605 Coe, H., Ng, N.L., Aiken, A.C., Docherty, K.S., Ulbrich, I.M., Grieshop, A.P., Robinson, A.L., Duplissy, J., Smith,
606 J.D., Wilson, K.R., Lanz, V.A., Hueglin, C., Sun, Y.L., Tian, J., Laaksonen, A., Raatikainen, T., Rautiainen, J.,
607 Vaattovaara, P., Ehn, M., Kulmala, M., Tomlinson, J.M., Collins, D.R., Cubison, M.J., Dunlea, E.J., Huffman, J.A.,
608 Onasch, T.B., Alfarra, M.R., Williams, P.I., Bower, K., Kondo, Y., Schneider, J., Drewnick, F., Borrmann, S.,
609 Weimer, S., Demerjian, K., Salcedo, D., Cottrell, L., Griffin, R., Takami, A., Miyoshi, T., Hatakeyama, S.,
610 Shimono, A., Sun, J.Y., Zhang, Y.M., Dzepina, K., Kimmel, J.R., Sueper, D., Jayne, J.T., Herndon, S.C., Trimborn,
611 A.M., Williams, L.R., Wood, E.C., Middlebrook, A.M., Kolb, C.E., Baltensperger, U., and Worsnop, D.R.,
612 Evolution of organic aerosols in the atmosphere, *Science*, 326 (5959), 1525-1529, **2009**.
613

614 Kanakidou, M., Seinfeld, J.H., Pandis, S.N., Barnes, I., Dentener, F.J., Facchini, M.C., Van Dingenen, R., Ervens,
615 B., Nenes, A., Nielsen, C.J., Swietlicki, E., Putaud, J.P., Balkanski, Y., Fuzzi, S., Horth, J., Moortgat, G.K.,
616 Winterhalter, R., Myhre, C.E.L., Tsigaridis, K., Vignati, E., Stephanou, E.G., and Wilson, J., Organic aerosol and
617 global climate modelling: A review, *Atmos. Chem. Phys.*, 5 (4), 1053-1123, **2005**.
618

619 Kelly, J., Makar, P.A., and Plummer, D. Projections of mid-century summer air-quality for North America: effects
620 of changes in climate and precursor emissions, *Atmos. Chem. Phys.*, 12, 5367-5390, **2012**.
621

622 Kroll, J.H., Ng, N.L., Murphy, S.M., Varutbangkul, V., Flagan, R.C., and Seinfeld, J.H., Chamber studies of
623 secondary organic aerosol growth by reactive uptake of simple carbonyl compounds, *J. Geophys. Res. Atmos.*, 110
624 (23), 1-10, **2005**.
625

626 Kroll, J.H. and Seinfeld, J.H., Chemistry of secondary organic aerosol: Formation and evolution of low-volatility
627 organics in the atmosphere, *Atmos. Environ.*, 42 (16), 3593-3624, **2008**.
628

629 Lee, P. and Ngan, F., Coupling of Important Physical Processes in the Planetary Boundary Layer between
630 Meteorological and Chemistry Models for Regional to Continental Scale Air Quality Forecasting: An Overview,
631 *Atmosphere*, 2, 464-483, **2011**.
632

633 Lelieveld, J., Evans, J.S., Fnais, M., Giannadaki, D., and Pozzer, A., The contribution of outdoor air pollution
634 sources to premature mortality on a global scale, *Nature*, 525 (7569), 367-371, **2015**.
635

636 Li, S.-M., Leithead, A., Moussa, S.G., Liggio, J., Moran, M.D., Wang, D., Hayden, K., Darlington, A., Gordon, M.,
637 Staebler, R., Makar, P.A., Stroud, C.A., McLaren, R., Liu, P.S.K., O'Brien, J., Mittermeier, R.L., Zhang, J., Marson,
638 G., Cober, S.G., Wolde, M., and Wentzell, J.J.B., Differences between measured and reported volatile organic
639 compound emissions from oil sands facilities in Alberta, Canada, *Proceedings of the National Academy of Sciences*
640 of the United States of America, 114 (19), pp. E3756-E3765, **2017**.
641

642 Liggio, J., Li, S.-M., and McLaren, R., Reactive uptake of glyoxal by particulate matter, *J. Geophys. Res. Atmos.*,
643 110 (10), 1-13, **2005**.
644

645 Liggio, J., Li, S.-M., Hayden, K., Taha, Y.M., Stroud, C., Darlington, A., Drollette, B.D., Gordon, M., Lee, P., Liu,
646 P., Leithead, A., Moussa, S.G., Wang, D., O'Brien, J., Mittermeier, R.L., Brook, J.R., Lu, G., Staebler, R.M., Han,
647 Y., Tokarek, T.W., Osthoff, H.D., Makar, P.A., Zhang, J., Plata, D.L., and Gentner, D.R., Oil sands operations as a
648 large source of secondary organic aerosols, *Nature*, 534 (7605), 91-94, **2016**.
649

650 Liggio, J., Stroud, C.A., Wentzell, J. *et al.*, Quantifying the primary emissions and photochemical formation of
651 isocyanic acid downwind of Oil Sands operations, *Environ. Sci. Technol.*, doi: 10.1021/acs.est.7b04346, **2017**.
652

653 Lopez-Hilfiker, F.D., F.D., Mohr, C., D'Ambro, E.L., Lutz, A., Riedel, T.P., Gaston, C.J., Iyer, S., Zhang, Z., Gold,
654 A., Surratt, J.D., Lee, B.H., Kurten, T., Hu, W.W., Jimenez, J., Hallquist, M., and Thornton, J.A., Molecular
655 composition and volatility of organic aerosol in the Southeastern U.S.: Implications for IEPOX Derived SOA,
656 *Environ. Sci. Technol.*, 50 (5), 2200-2209, **2016**.
657

658 Ma, P. K., Zhao, Y., Robinson, A. L., Worton, D. R., Goldstein, A. H., Ortega, A. M., Jimenez, J. L., Zotter, P.,
659 Prévôt, A. S. H., Szidat, S., and Hayes, P. L.: Evaluating the impact of new observational constraints on P-S/IVOC
660 emissions, multigeneration oxidation, and chamber wall losses on SOA modeling for Los Angeles, CA, *Atmos.*
661 *Chem. Phys.*, 17, 9237–9259, **2017**.
662

663 Makar, P.A., Gong, W., Milbrandt, J., Hogrefe, C., Zhang, Y., Curci, G., Žabkar, R., Im, U., Balzarini, A., Baró, R.,
664 Bianconi, R., Cheung, P., Forkel, R., Gravel, S., Hirtl, M., Honzak, L., Hou, A., Jiménez-Guerrero, P., Langer, M.,
665 Moran, M.D., Pabla, B., Pérez, J.L., Pirovano, G., San José, R., Tuccella, P., Werhahn, J., Zhang, J., and Galmarini,
666 S., Feedbacks between air pollution and weather, Part 1: Effects on weather, *Atmos. Environ.*, 115, 442-469, **2015a**.
667

668 Makar, P.A., Gong, W., Hogrefe, C., Zhang, Y., Curci, G., Žabkar, R., Milbrandt, J., Im, U., Balzarini, A., Baró, R.,
669 Bianconi, R., Cheung, P., Forkel, R., Gravel, S., Hirtl, M., Honzak, L., Hou, A., Jiménez-Guerrero, P., Langer, M.,
670 Moran, M.D., Pabla, B., Pérez, J.L., Pirovano, G., San José, R., Tuccella, P., Werhahn, J., Zhang, J., and Galmarini,
671 S., Feedbacks between air pollution and weather, part 2: Effects on chemistry, *Atmos. Environ.*, 115, 499-526,
672 **2015b**.
673

674 Makar, P.A. *et al.*, Estimates of Exceedances of Critical Loads for Acidifying Deposition in Alberta and
675 Saskatchewan, accepted in *ACP*, **2018**.
676

677 Mashayekhi, R., Zhao, S., Saeednooran, S., Hakami, A., Ménard, R., Moran, M. D., and Zhang, J., Emissions
678 Uncertainty Inventory and Modeling Framework: Case Study of Residential Wood Combustion, 15th Annual
679 CMAS Conference, October 24-26, Chapel Hill, NC,
680 https://www.cmascenter.org/conference//2016/slides/mashayekhi_development_emission_2016.pptx, **2016**.
681

682 McNeill, V.F., Aqueous organic chemistry in the atmosphere: Sources and chemical processing of organic aerosols,
683 *Environ. Sci. Technol.*, 49 (3), 1237-1244, **2015**.
684

685 Moran, M.D., Ménard, S., Pavlovic, R., Anselmo, D., Antonopoulos, S., Makar, P.A., Gong, W., Gravel, S., Stroud,
686 C., Zhang, J., Zheng, Q., Robichaud, A., Landry, H., Beaulieu, P.A., Gilbert, S., Chen, J., and Kallaur, A., Recent
687 Advances in Canada's National Operational AQ Forecasting System, NATO Science for Peace and Security Series
688 C: Environmental Security, 137, 215-220, **2013**.

689
690 Office of the Federal Register National Archives and Records Administration, Protection of Environment, Code of
691 Federal Regulations, Title 40, Parts 50 to 51, Special Edition of the Federal Register, U.S. government publishing
692 office, Washington, DC 20402-0001, July 1, **2015**.
693
694 Pankow, J.F., An absorption model of the gas/aerosol partitioning involved in the formation of secondary organic
695 aerosol, *Atmos. Environ.*, 28 (2), 189-193, **1994**.
696
697 Park, S.H., Gong, S.L., Bouchet, V.S., Gong, W., Makar, P.A., Moran, M.D., Stroud, C.A., and Zhang, J.,
698 Effects of black carbon aging on air quality predictions direct radiative forcing estimation, *Tellus, Series B:*
699 *Chemical and Physical Meteorology*, 63 (5), 1026-1039, **2011**.
700
701 Pouliot, G., Pierce, T., Denier van der Gon, H., Schaap, M., Moran, M., and Nopmongcol, U., Comparing emission
702 inventories and model-ready emission datasets between Europe and North America for the AQMEII project, *Atmos.*
703 *Environ.*, 53, 4-14, **2012**.
704
705 Pouliot, G., Denier van der Gon, H.A.C., Kuenen, J., Zhang, J., Moran, M.D., and Makar, P.A., Analysis of the
706 emission inventories and model-ready emission datasets of Europe and North America for phase 2 of the AQMEII
707 project, *Atmos. Environ.*, 115, 345-360, **2015**.
708
709 Robinson, A.L., Donahue, N.M., Shrivastava, M.K., Weitkamp, E.A., Sage, A.M., Grieshop, A.P., Lane, T.E.,
710 Pierce, J.R., and Pandis, S.N., Rethinking organic aerosols: Semivolatile emissions and photochemical aging,
711 *Science*, 315 (5816), 1259-1262, **2007**.
712
713 Rouleau, M., Egyed, M., Taylor, B., Chen, J., Samaali, M., Davignon, D., and Morneau, G., Human health impacts
714 of biodiesel use in on-road heavy duty diesel vehicles in Canada, *Environ. Sci. Technol.*, 47 (22), 13113-13121,
715 2013.
716
717 Schultz, M.G., Diehl, T., Brasseur, G.P., and Zittel, W., Air Pollution and Climate-Forcing Impacts of a Global
718 Hydrogen Economy, *Science*, 302 (5645), 624-627, **2003**.
719
720 Seinfeld, J. H. and Pandis, S. N., *Atmospheric Chemistry and Physics from air pollution to climate change*, New
721 York. John Wiley and Sons, Incorporated, **1998**.
722
723 Shrivastava, M., Easter, R.C., Liu, X., Zelenyuk, A., Singh, B., Zhang, K., Ma, P.-L., Chand, D., Ghan, S., Jimenez,
724 J.L., Zhang, Q., Fast, J., Rasch, P.J., and Tiitta, P., Global transformation and fate of SOA: Implications of low-
725 volatility SOA and gas-phase fragmentation reactions, *J. Geophys. Res.*, 120 (9), 4169-4195, **2015**.
726
727 Slowik, J.G., Stroud, C., Bottenheim, J.W., Brickell, P.C., Chang, R.Y.-W., Liggio, J., Makar, P.A., Martin, R.V.,
728 Moran, M.D., Shantz, N.C., Sjostedt, S.J., Van Donkelaar, A., Vlasenko, A., Wiebe, H.A., Xia, A.G., Zhang, J.,
729 Leaitch, W.R., and Abbatt, J.P.D., Characterization of a large biogenic secondary organic aerosol event from eastern
730 Canadian forests, *Atmos. Chem. Phys.*, 10 (6), 2825-2845, **2010**.
731
732 Solazzo, E., Bianconi, R., Pirovano, G., Matthias, V., Vautard, R., Moran, M.D., Wyatt Appel, K., Bessagnet, B.,
733 Brandt, J., Christensen, J.H., Chemel, C., Coll, I., Ferreira, J., Forkel, R., Francis, X.V., Grell, G., Grossi, P.,
734 Hansen, A.B., Miranda, A.I., Nopmongcol, U., Prank, M., Sartelet, K.N., Schaap, M., Silver, J.D., Sokhi, R.S., Vira,
735 J., Werhahn, J., Wolke, R., Yarwood, G., Zhang, J., Rao, S.T., and Galmarini, S., Operational model evaluation for
736 particulate matter in Europe and North America in the context of AQMEII, *Atmos. Environ.*, 53, 75-92, **2012**.
737
738 Stroud, C. A., Morneau, G., Makar, P. A., Moran, M. D., Gong, W., Pabla, B., Zhang, J., Bouchet, V. S., Fox, D.,
739 Venkatesh, S., Wang, D., and Dann, T., OH-reactivity of volatile organic compounds at urban and rural sites across
740 Canada: Evaluation of air quality model predictions using speciated VOC measurements, *Atmos. Environ.*, 42,
741 7746-7756, **2008**.
742

743 Stroud, C.A., Makar, P.A., Moran, M.D., Gong, W., Gong, S., Zhang, J., Hayden, K., Mihele, C., Brook, J.R.,
744 Abbatt, J.P.D., and Slowik, J.G., Impact of model grid spacing on regional- and urban- scale air quality predictions
745 of organic aerosol, *Atmos. Chem. Phys.*, 11 (7), 3107-3118, **2011**.
746
747 Stroud, C.A., Zaganescu, C., Chen, J., McLinden, C.A., Zhang, J., and Wang, D., Toxic volatile organic air
748 pollutants across Canada: multi-year concentration trends, regional air quality modelling and source apportionment,
749 *J. Atmos. Chem.*, 73 (2), 137-164, **2016**.
750
751 Tunved, P., Hansson, H.-C., Kerminen, V.-M., Ström, J., Maso, M.D., Lihavainen, H., Viisanen, Y., Aalto, P. P.,
752 Komppula, M., and Kulmala, M., High natural aerosol loading over boreal forests, *Science*, 312, 261–263,
753 doi:10.1126/science.1123052, **2006**.
754
755 Wang, X., Chow, J. C., Kohl, S. D., Percy, K. E., Legge, A. H., and Watson, J. G., Characterization of PM_{2.5} and
756 PM₁₀ fugitive dust source profiles in the Athabasca Oil Sands Region, *Journal of the Air & Waste Management*
757 *Association*, 65:12, 1421-1433, DOI: 10.1080/10962247.2015.1100693, **2015**.
758
759 Zhang, J., Zheng, Q., Moran, M. D., Makar, P. A., Akingunola, A., Li, S.-M., Marson, G., Gordon, M., Melick, R.,
760 and Cho, S., Emissions preparation for high-resolution air quality modelling over the Athabasca oil sands region of
761 Alberta, Canada, 21st Intern. Emissions Inventory Conference, 13-17 April, San Diego,
762 http://www.epa.gov/ttn/chief/conference/ei21/session1/zhang_emissions.pdf, 18 pp, **2015**.
763
764 Zhang, J. *et al.*, Emissions preparation and analysis for Multiscale Air Quality Modelling over the Athabasca Oil
765 Sands Region of Alberta, Canada, accepted in *ACP*, **2018**.
766
767
768
769
770
771
772
773
774
775
776
777
778
779
780
781
782
783
784
785
786
787
788
789
790
791
792
793
794
795
796
797
798

799 **Table 1. Facility total emission rates for three lumped organic species and PM_{2.5} calculated**
 800 **with the bottom-up, base case inventory, CEMA facility-specific VOC profiles (labeled**
 801 **Base Case) and the top-down measurement-derived rates (labeled Revised Emission case,**
 802 **scaled to tonnes/year for VOCs or tonnes/Aug&Sept for PM_{2.5}). Emission rate**
 803 **increase/decrease of more than ±500 tonnes compared to base case is shown in red/blue.**

Species	Suncor – M/S		Syncrude - ML		Shell – MR/J		CNRL - Horizon	
	Base Case	Revised	Base Case	Revised	Base Case	Revised	Base Case	Revised
Mono-Substituted Aromatics (TOLU)	486	1112	806	1539	6.8	72	135	393
Multi-Substituted Aromatics (AROM)	1457	1569	5273	1696	746	88	1125	500
Long Chain Alkanes (ALKA)	5636	13488	12348	10022	1690	14384	2651	23779
Particulate Matter (PM_{2.5})	1251	2537*	1021	3648*	459	2423*	402	1015*

804 VOC revised-emissions are based on annual estimates, derived in Li *et al.*, (2017). The estimates
 805 consider monthly and annual oil production yields reported by facilities for the plant stack
 806 emissions. For tailing ponds and mine faces, the VOC estimates are calculated using a surface-
 807 to-atmosphere mass transfer model considering ambient temperature and wind speed.

808 * PM_{2.5} revised emissions are based on 2-month emission (Aug&Sept) rather than based on an
 809 annual estimate (Zhang *et al.*, 2018) due to uncertainties in calculating dust emissions in the
 810 winter months.

811
812
813
814
815
816
817
818
819
820
821
822
823
824
825
826
827
828
829
830
831

832 **Table 2. Facility-specific VOC speciation profiles (mass fractions) applied to the surface**
 833 **mining facilities in the Athabasca oil sands region compared to standard speciation profiles**
 834 **for Canadian and U.S. petrochemical oil refineries (in ADOM-II chemical speciation). Data**
 835 **are based on Zhang *et al.* (2018) and references therein. All four profiles are used in the**
 836 **base case simulation.**

Species	Shell M/J, Syncrude AN, Imperial Kearn Base Case Plant Profile (CEMA)	Syncrude ML, Suncor, CNRL Base Case Plant Profile (CEMA)	CEPS Database Standard Profile #9012 For Oil Refineries in Base Case	SPECIATE Database Standard Profile #0316 For Oil Refineries in Base Case
EC38 (Propane, Benzene, Acetylene)	0.0	0.0	0.247	0.176
EA3 (Alkane ≥C4)	0.90	0.71	0.623	0.781
EA2 (Alkene ≥C3)	0.007	0.069	0.031	0.002
ETOL (Toluene and other mono- aromatics)	0.001	0.057	0.005	0.008
EARO (Multi- functional aromatics)	0.0003	0.099	0.003	0.003
EHCO (Formaldehyde)	0.00001	0.0003	0.110	0.0

837 Columns do not add up to unity due to “unaccounted for” or “unassigned species” and/or due to
 838 consideration of reactivity weighting for the ADOM-II mechanism.

839
 840 Refinery Profile #9012 is a profile from the Canadian Emissions Processing System (Moran,
 841 M.D., M.T. Scholtz, C.F. Slama, A. Dorkalam, A. Taylor, N.S. Ting, D. Davies, P.A. Makar, S.
 842 Venkatesh, An Overview of CEPS1.0: Version 1.0 of the Canadian Emissions Processing
 843 System for Regional-Scale Air Quality Models. In Proc. 7th AWMA Emission Inventory Symp.,
 844 Research Triangle Park, North Carolina, Air & Waste Management Association, Pittsburgh, Oct.
 845 28-30, 1997.)

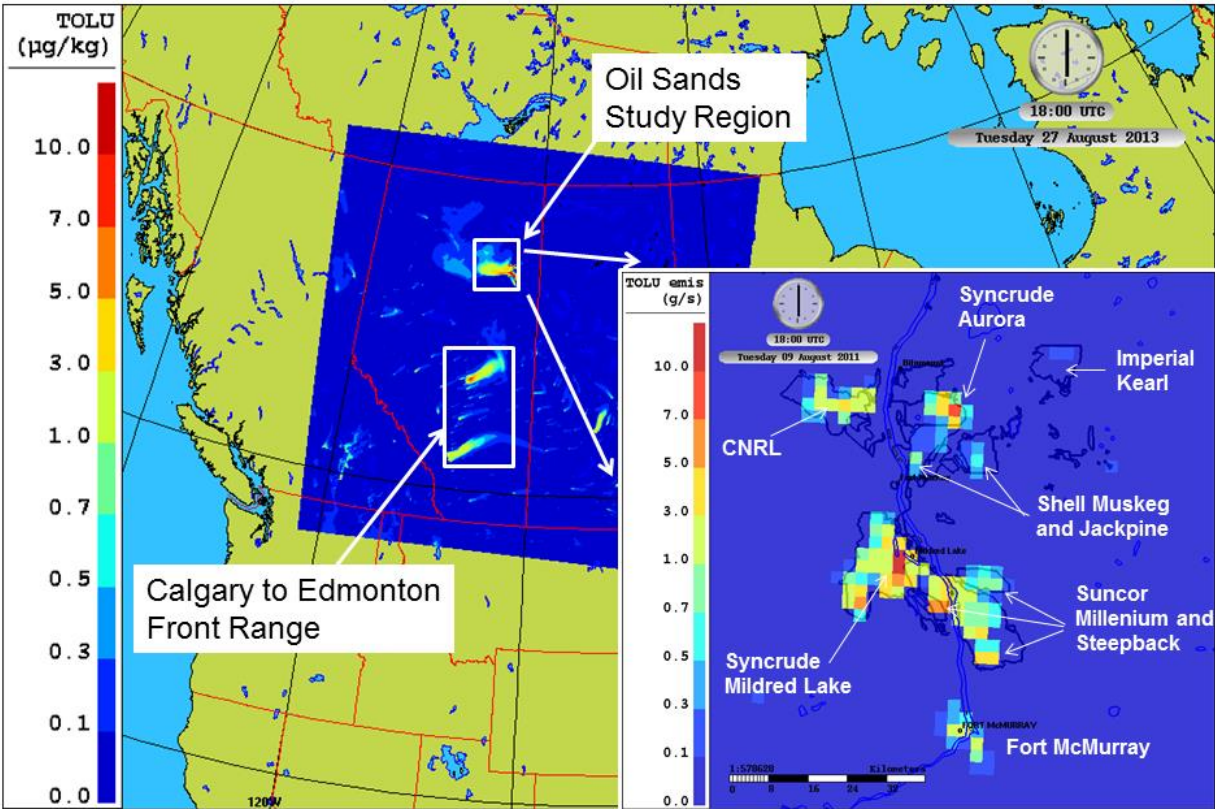
846
 847
 848
 849
 850
 851
 852

853 **Table 3. Statistical scores from the model simulations with revised and base case**
 854 **emissions; all statistics are relative to observations.**

Lumped Species	Simulation	Mean Bias (ppbv)	RMSE (ppbv)	Slope	Y-intercept (ppbv)	Correlation Coefficient, R
TOLU	Base Case	-0.041	0.277	0.217	0.063	0.32
	Revised Emissions	0.049	0.386	0.426	0.125	0.31
AROM	Base Case	0.152	0.435	0.957	0.154	0.41
	Revised Emissions	0.044	0.227	0.383	0.083	0.37
ALKA	Base Case	-0.123	5.556	0.378	2.028	0.24
	Revised Emissions	1.98	6.403	0.335	4.097	0.34
OA	Base Case	-2.79	3.866	0.186	0.252	0.59
	Revised Emissions	-2.37	3.632	0.292	0.273	0.49

855 RMSE is the root mean square error. Y-intercept corresponds to the model intercept of a model
 856 vs observation correlation plot. Mean bias is the model-observation mean score. The better score
 857 for a given pair of statistics is shown in **bold-face** font.

858
 859
 860
 861
 862
 863
 864
 865
 866
 867
 868
 869
 870
 871
 872
 873
 874
 875
 876
 877
 878
 879
 880
 881
 882
 883
 884
 885
 886
 887
 888
 889
 890
 891
 892



893

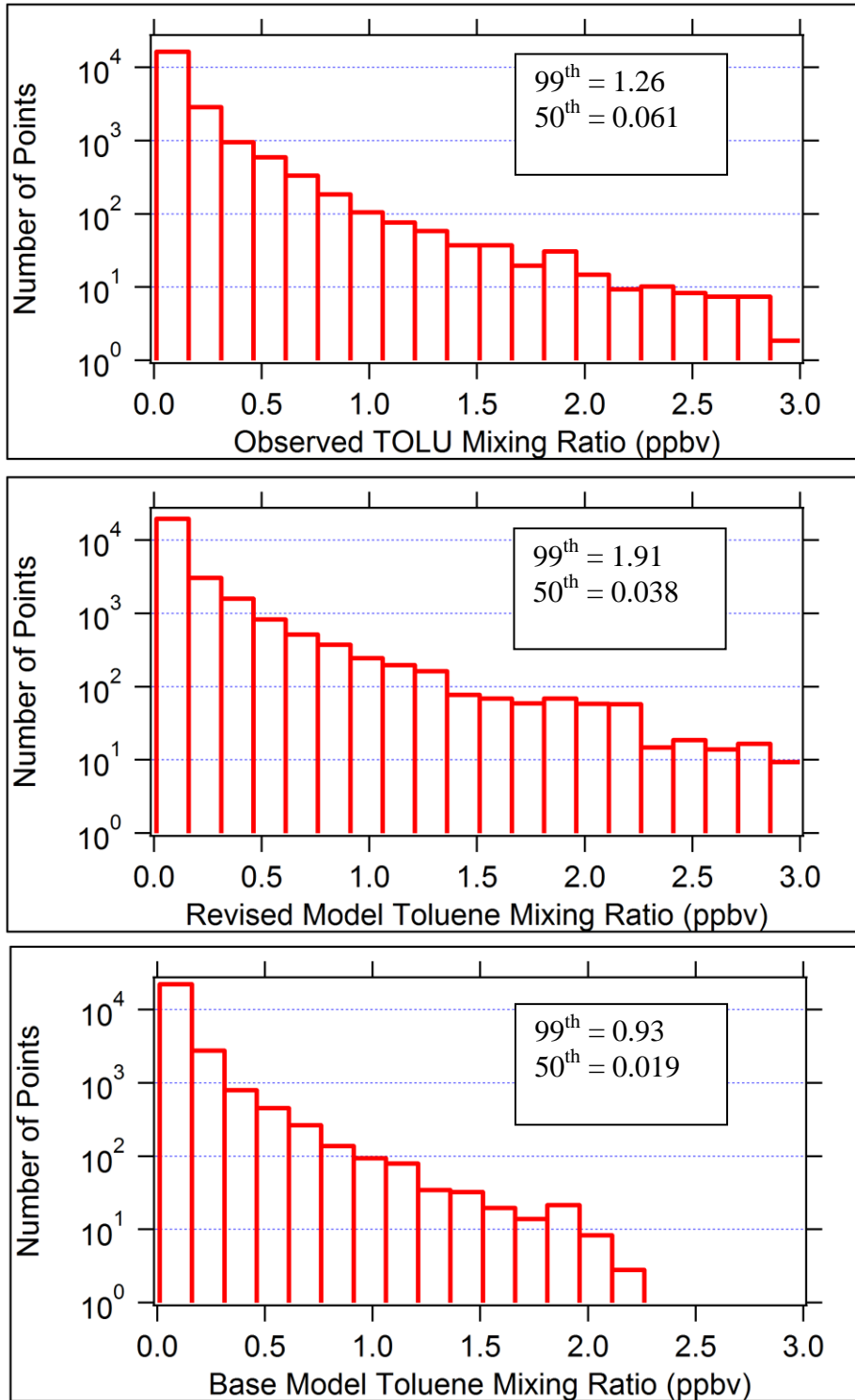
894 Figure 1. The background image is the nested domain, at 2.5-km grid spacing, covering all of
 895 Alberta and Saskatchewan and encompassing the Athabasca Oil Sand study region (white box).
 896 The model field shown is for the lumped toluene species (TOLU) mass mixing ratio ($\mu\text{g}/\text{kg}$ air).
 897 The inserted image on the right is the TOLU emission map ($\text{g}/\text{s}/\text{grid cell}$) for the Oil Sands study
 898 region at the same hour as mixing ratio image on the left. The Oil Sand facility's names are
 899 listed in white labels.

900

901

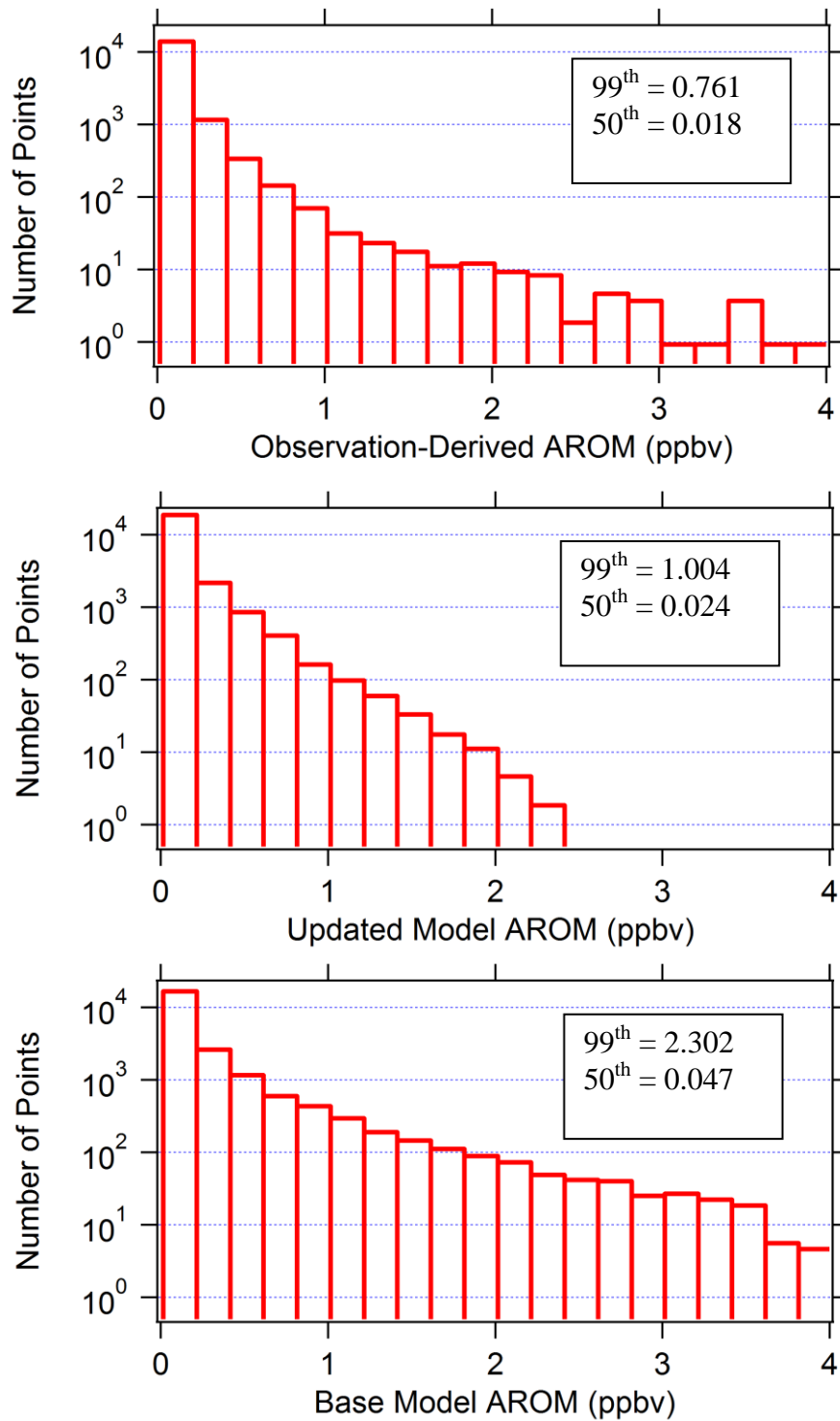
902

903



904

905 Figure 2. Histograms for (a) observed TOLU, (b) revised-emissions TOLU, and (c) base-case-
 906 emissions TOLU volume mixing ratios (ppbv). Points correspond to 10-sec averaged aircraft and
 907 model data, sorted into 20 bins by volume mixing ratio. The inset boxes show the 50th and 99th
 908 percentile values for each histogram.



909

910 Figure 3. Histograms for (a) observed AROM, (b) revised-emissions AROM, and (c) base model AROM
 911 volume mixing ratios (ppbv). Points correspond to 10-sec averaged aircraft and model data, sorted into
 912 20 bins by volume mixing ratio. The inset boxes show the 50th and 99th percentile values for each
 913 histogram

914

915

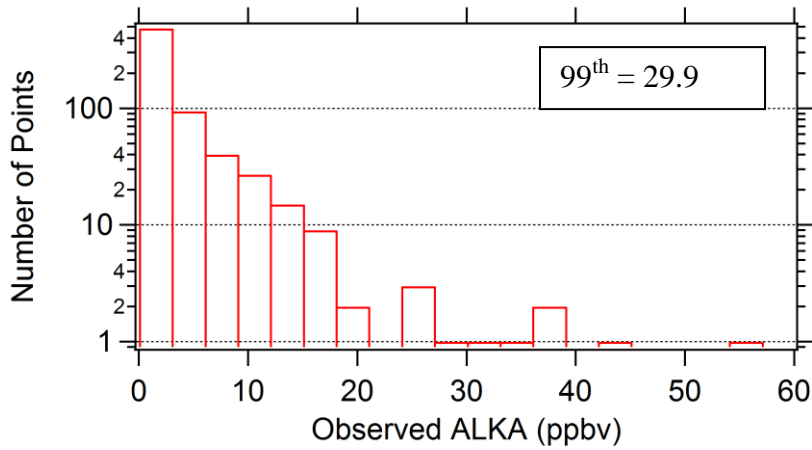
916

917

918

919

920



921

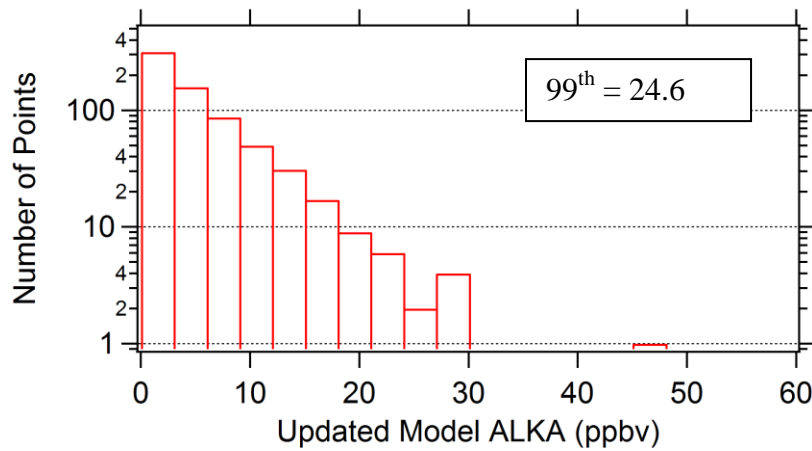
922

923

924

925

926



927

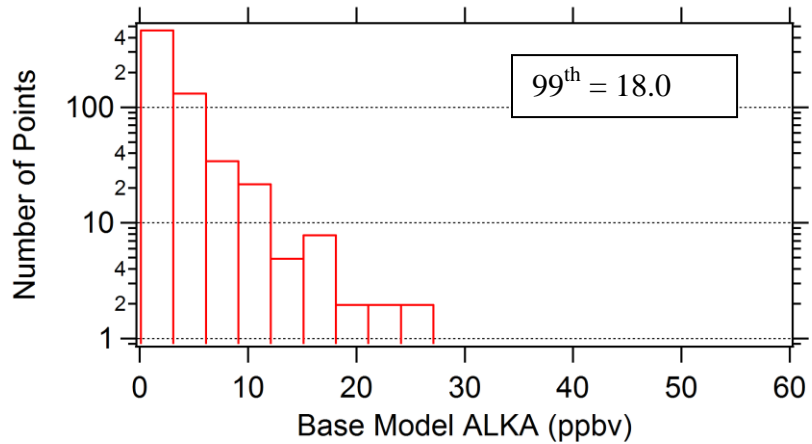
928

929

930

931

932



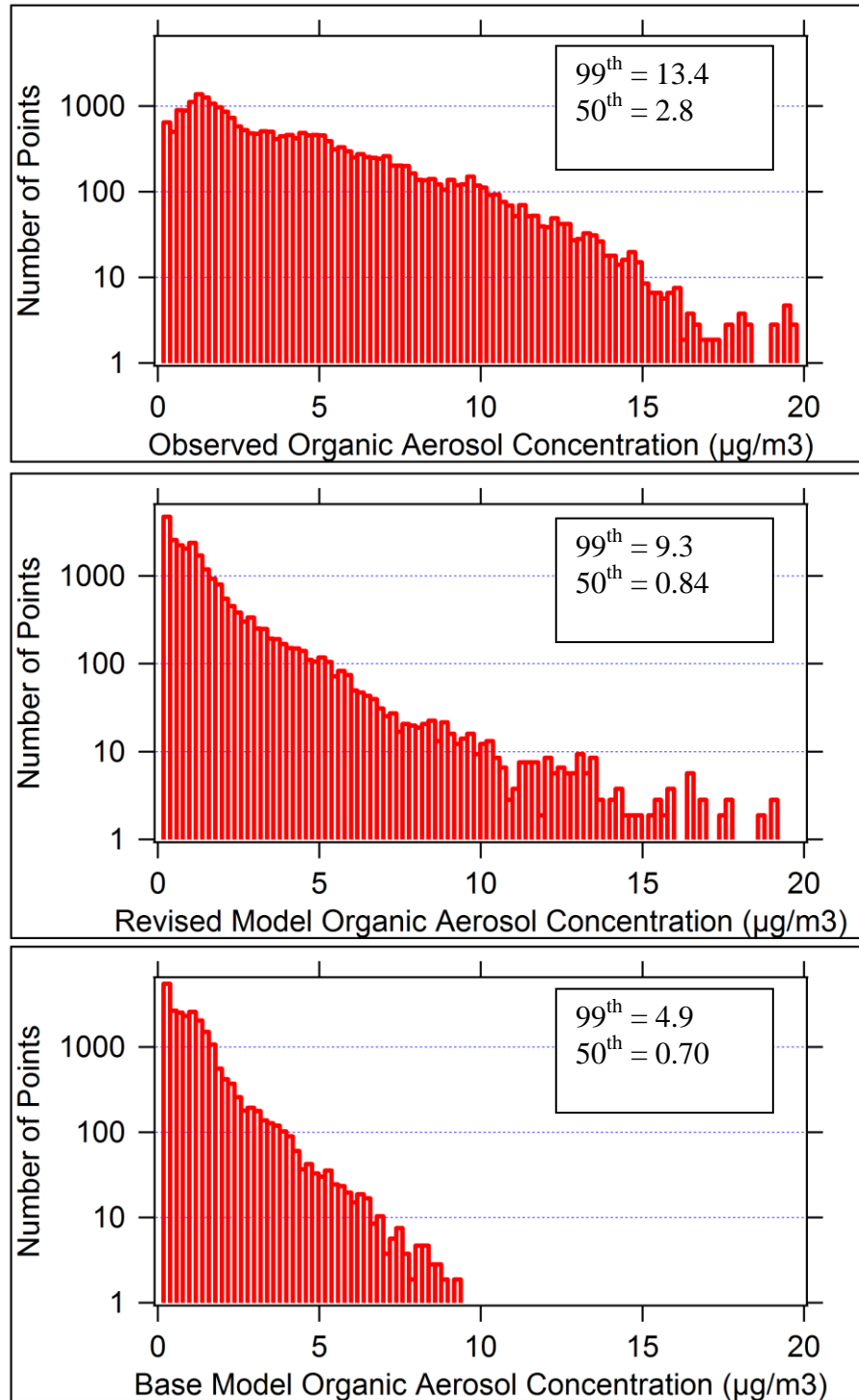
933

934

935 Figure 4. Histograms for (a) observed ALKA, (b) revised-emissions ALKA, and (c) base-case emissions
936 ALKA volume mixing ratios (ppbv). Points correspond to canister grab samples and model data,
937 sorted into 20 bins by mixing ratio. The inset boxes show the 99th percentile value for each
938 histogram.

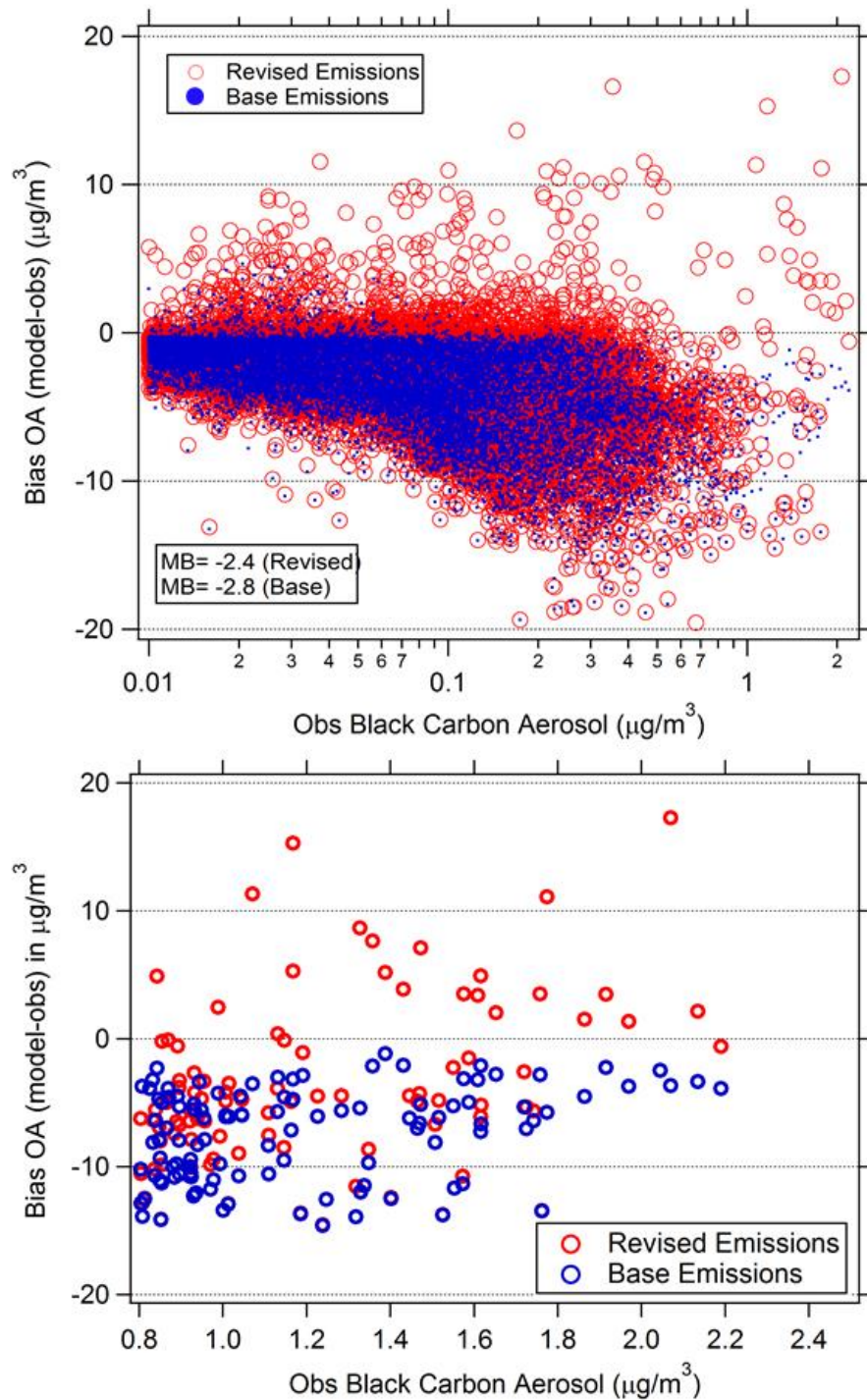
939

940



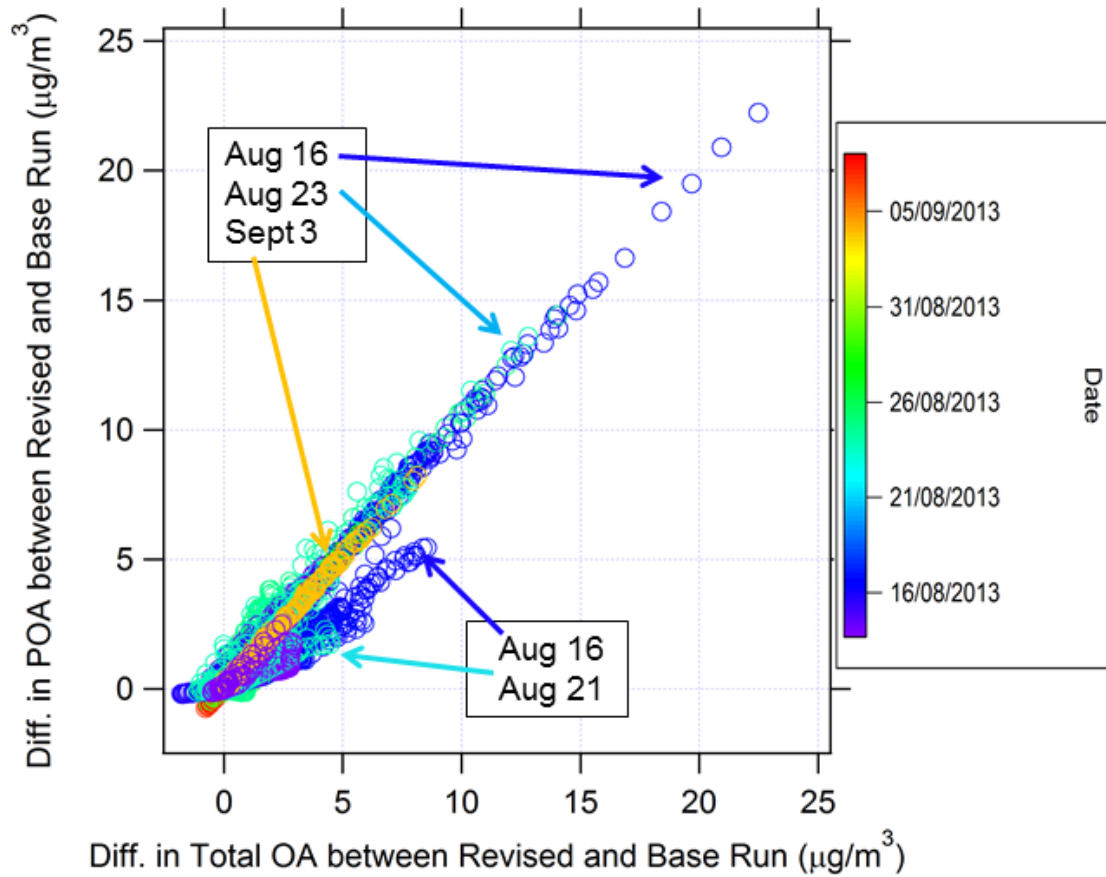
941

942 Figure 5. Histograms for (a) observed organic aerosol (OA), (b) revised-emissions OA, and (c) base-
 943 case emissions OA concentrations ($\mu\text{g}/\text{m}^3$). Points correspond to 10-sec averaged aircraft and model
 944 data. The inset boxes show the 50th and 99th percentile values for each histogram.



945

946 Figure 6ab. Organic aerosol model bias as a function of observed black carbon aerosol. The
 947 bottom panel is an enlargement of the upper panel showing only the data points for observed
 948 BC > 0.8 $\mu\text{g}/\text{m}^3$. The model results for the base-case emissions run are plotted in blue and points
 949 in red correspond to the revised-emissions run. The data plotted is for all the aircraft flights.



950

951 Figure 7. Difference in predicted POA concentrations between revised-emissions and base-case
 952 runs plotted as a function of the difference in predicted total OA concentration between the
 953 revised-emissions and base-case runs for all flights. Points along the 1:1 line show a difference
 954 solely from POA emission changes. Points below the 1:1 line show enhanced SOA formation.